RESEARCH ARTICLE

BIOENGINEERING &
TRANSLATIONAL MEDICINE

Assessment of human adipose-derived stem cell on surface-modified silicone implant to reduce capsular contracture formation

Chanutchamon Sutthiwanjampa[1] | Byung Ho Shin[2] | Na Eun Ryu[1] |
Shin Hyuk Kang[3] | Chan Yeong Heo[2,4,5,6] | Hansoo Park[1] 🔘

[1]School of Integrative Engineering, Chung-Ang University, Seoul, Republic of Korea

[2]Department of Biomedical Engineering, College of Medicine, Seoul National University, Seoul, Republic of Korea

[3]Department of Plastic and Reconstructive Surgery, Chung-Ang University Hospital, Seoul, Republic of Korea

[4]Department of Plastic and Reconstructive Surgery, Seoul National University Bundang Hospital, Seongnam, Republic of Korea

[5]Interdisciplinary Program for Bioengineering, College of Engineering, Seoul National University, Seoul, Republic of Korea

[6]Department of Plastic and Reconstructive Surgery, College of Medicine, Seoul National University, Seoul, Republic of Korea

Correspondence

Chan Yeong Heo, Department of Biomedical Engineering, College of Medicine, Seoul National University, 101 Daehak-ro, Ihwa-dong, Jongno-gu, Seoul 03080, Republic of Korea.
Email: lionheo@gmail.com

Hansoo Park, School of Integrative Engineering, Chung-Ang University, 84 Heukseok-ro, Heukseok-dong, Dongjak-gu, Seoul 06974, Republic of Korea.
Email: heyshoo@cau.ac.kr

Funding information

Ministry of Science and ICT, South Korea, Grant/Award Numbers: NRF-2018M3D1A1058813, NRF-2021R1A2C2007189

Abstract

Medical devices made from poly(dimethylsiloxane) (PDMS)-based silicone implants have been broadly used owing to their inert properties, biocompatibility, and low toxicity. However, long-term implantation is usually associated with complications, such as capsular contracture due to excessive local inflammatory response, subsequently requiring implant removal. Therefore, modification of the silicone surface to reduce a risk of capsular contracture has attracted increasing attention. Human adipose-derived stem cells (hASCs) are known to provide potentially therapeutic applications for tissue engineering, regenerative medicine, and reconstructive surgery. Herein, hASCs coating on a PDMS (hASC-PDMS) or itaconic acid (IA)-conjugated PDMS (hASC-IA-PDMS) surface is examined to determine its biocompatibility for reducing capsular contracture on the PDMS surface. In vitro cell cytotoxicity evaluation showed that hASCs on IA-PDMS exhibit higher cell viability than hASCs on PDMS. A lower release of proinflammatory cytokines is observed in hASC-PDMS and hASC-IA-PDMS compared to the cells on plate. Multiple factors, including in vivo mRNA expression levels of cytokines related to fibrosis; number of inflammatory cells; number of macrophages and myofibroblasts; capsule thickness; and collagen density following implantation in rats for 60 days, indicate that incorporated coating hASCs on PDMSs most effectively reduces capsular contracture. This study demonstrates the potential of hASCs coating for the modification of PDMS surfaces in enhancing surface biocompatibility for reducing capsular contracture of PDMS-based medical devices.

KEYWORDS

antifibrotic property, capsular contracture, foreign body response, human adipose-derived stem cells, itaconic acid, poly(dimethylsiloxane), surface conjugation

1 | INTRODUCTION

Poly(dimethylsiloxane) (PDMS)-based silicone implants have been used in breast augmentation, rhinoplasty, and postmastectomy reconstruction in the plastic and reconstructive surgery fields for several decades. Recipients are usually satisfied with the tissue-like mechanical properties of silicone-based implants; however, their limited biocompatibility poses a challenge. For example, the surfaces of silicone breast implants have substantial limitations owing to the formation of a constrictive fibrotic capsule (known as capsular contracture) following implantation, which in addition to esthetic malfunction, has been shown to cause illness and deformation.[1] It has been reported that capsular contracture occurs over time ranging from months to years postimplantation.[2–5] Capsular contracture has been hypothesized to be caused by excessive foreign body reactions on silicone surfaces. Notably, capsule formation is a normal response to foreign bodies, whereas contracture is not. The formation of capsular contracture seems to be a multifactorial process. Immunological reactions of the patient to foreign bodies due to silicone gel leakage, dust, or powdered gloves, exaggerated inflammatory responses to foreign prosthetic materials, and bacterial inoculation and biofilm formation within the implant have been proposed as pathomechanisms underlying capsular contracture.[6–9] To overcome these challenges, current research has focused on the surface modification of prosthetic materials. A recent study reported the potential use of surface-modified implants to reduce capsular fibrosis via a local antifibrotic effect based on modifying the surface of silicone implants with halofuginone, an antifibrotic drug; this implant was found to decrease host responses to foreign bodies.[10] The areas of focus in research on the modification of silicone implant surfaces include increasing the hydrophilicity and biocompatibility of the surface and reducing excessive host reactions to foreign bodies. The surface wettability of any polymer can be improved by increasing its hydrophilicity, thereby enhancing its biocompatibility.[11]

Among the methods used to prepare biocompatible surfaces, surface coating with biomembrane-mimicking materials is considered the most desirable. Previously, successfully synthesized biomembrane-mimicking polymers with various phospholipid head groups have been reported.[12] These new biomembrane-mimicking polymers could be used in various application platforms in biomedical fields, such as tissue engineering or bioimplantation, in the near future. Itaconic acid (IA) is an organic compound known to be microbe-resistant, chemically reactive, biodegradable, biocompatible, and nontoxic.[13] It has been suggested to have excellent potential in a wide range of scientific fields, such as agricultural, food, pharmaceutical, biomedical, and other industries.[14] The two carboxyl groups of IA contribute to its hydrophilic property. IA has applications in wound healing, coat formation, water uptake, drug transport, and hydrogel forming[15–19]; in addition, it blocks isocitrate lyase, the primary enzyme of the glyoxylate shunt, a key pathway for bacterial growth under specific conditions.[20] In our recent studies, PDMS conjugated with 150 mM IA and 0.50 wt% IA-gelatin polymer demonstrated excellent and effective anti-protein adhesion, antibacterial adhesion, and in vivo anti-fibrotic functions.[21,22]

In recent years, various stem cells, such as T cells, hematopoietic stem cells, human adipose-derived stem cells (hASCs), and induced pluripotent stem cells, have attracted considerable attention regarding their applications in biomedical fields and have been favorable candidates for regenerative medicine, cell therapy, and cell engineering.[23] Among the stem cells using in biomedical therapy, hASCs have gained great interest in cell-based therapeutic applications in regenerative medicine and tissue engineering.[24] These stem cells can differentiate along multiple mesodermal, myogenic, and nonmesodermal lineages, such as adipogenic, osteogenic, muscle, and epithelial cells.[25] The isolation of hASCs from a stromal vascular fraction of adipose tissue is relatively easier than the isolation of other stem cells, and hence, small amounts of adipose tissue can yield a large number of stem cells compared with that from other sources.[25] In particular, hASCs are a miscellaneous population of cells and owing to their inherent multipotency and ability to enhance vascularization and adipogenesis, which makes them superior to other materials, they are known to have a broad range of potential therapeutic applications and thus represent a favorable cell-based therapeutic tool for tissue engineering, regenerative medicine, and reconstructive surgery.[26,27] Based on these findings, autologous adipose tissue or adipose tissue with hASCs has been used for breast reconstruction in patients with breast cancer who have undergone mastectomy.[28,29] Moioli et al. reported that hASCs regenerated functional, highly vascularized adipose tissue following transplantation in a murine xenograft model.[30] Additionally, hASCs have been reported to possess important immunoregulatory effects via paracrine signaling,[31] including immunosuppressive effects on several immune cells under varying conditions,[32,33] and protect tissue against ischemia–reperfusion injury, thereby increasing tissue survival.[25] Moreover, hASCs have been applied to various medical devices to enhance biocompatibility for application in many medical fields, such as dental implants[23] and osteogenesis.[34,35] Many alternative approaches have focused on using hASCs to reduce fibrosis and capsular contracture over the last decades.[36–39] Recently, Thomé et al. found that hASC-enriched fat grafting could successfully reduce capsular contracture formation in rats.[40] Further, various silicone surface modification techniques have been used to reduce the complications from silicone-based medical devices.[23,34,41–45] Nevertheless, few studies have researched silicone implant surface modification using hASCs to reduce breast capsular contraction. Barr et al. reported that a biomimetic breast adipose tissue-derived breast implant surface could effectively decrease the inflammatory phase of the implant-driven foreign body reaction related to capsular contracture in vitro.[36] However, to the best of our knowledge, no previous research has investigated the surface modification of silicone implants using hASCs to reduce capsular contracture in vivo. We therefore used hASCs, according to their multipotency, to modify a PDMS surface by coating them on the surface of bare PDMS or IA-conjugated PDMS (IA-PDMS), a hydrophilic modified-surface developed in our previous studies.[21,22] We aimed to evaluate and compare the ability of IA-PDMS, hASC-coated PDMS (hASC-PDMS), and hASC-coated IA-PDMS (hASC-IA-PDMS) to reduce the formation of capsular contracture. We hypothesized that hASC-IA-PDMS could most efficiently reduce the formation of capsular contracture following silicone implantation.

2 | RESULTS AND DISCUSSION

2.1 | Preparation of IA-PDMS

PDMS was prepared by mixing the base and curing agent at 10:1 (w/w), which was reported as the best ratio for biological application[46,47] and has been used as a model of silicone implants in several studies.[48–52] We chemically modified the surface of PDMS with 150 mM IA (Figure 1). This concentration was selected because previously, it was reported to result in the excellent enhancement of biocompatibility and reduction in capsular contracture formation of the PDMS surface, similar to results with the 0.50 wt% IA-GT polymer but with an easier preparation method than the latter.[21,22] Measurement of the water contact angle and the attenuated total reflectance/Fourier transform infrared (ATR/FTIR) spectra was used to confirm the formation of IA on the PDMS surface. As shown in Figure S1a, the contact angle was significantly decreased from $96.74 \pm 5.998°$ to $35.66 \pm 3.552°$ following IA conjugation ($p < 0.0001$), indicating an improvement in the wettability of the PDMS surface, resulting in hydrophilicity owing to the presence of IA. Additionally, this was confirmed in Figure S2a, which illustrates the formation of IA based on the appearance of the peak at 1650 cm^{-1} and 1548 cm^{-1}, indicating C=O and C—N groups, respectively. More specifically, C=O stretching was introduced by IA, whereas the C—N bonding indicates the formation of an amide.[21]

2.2 | Characterization of human adipose-derived stem cells and investigation of cell viability, morphology, and adhesion patterns

We then characterized the phenotype of hASCs via fluorescence-activated cell sorting analysis in accordance with the low expression of surface makers including CD14, CD34, and CD45 and high expression of major surface marker including CD73 and CD105.[53–56] As predicted, high expression of CD73 and CD105 and low expression of CD14, CD34, and CD45 were observed (Figure S3), consistent with that in prior studies.[53,57,58] To observe cell viability and the adhesion pattern of hASCs grown on a culture plate, PDMS, and IA-PDMS, the Live/Dead assay was used. This assay showed that the viability of cells on IA-PDMS surfaces was better than that on a PDMS surface and comparable to that on a culture plate (control) at 1, 3, and 7 days (Figure 2a). We also observed the morphology of cells grown on a culture plate, PDMS, and IA-PDMS using rhodamine/DAPI (4',6-diamidino-2-phenylindole) staining. Accordingly, the morphology of cells cultured on an IA-PDMS surface was similar to that on a culture plate at 1, 3, and 7 days (Figure 2b). However, the morphology of cells cultured on PDMS surfaces appeared more round-shaped than those grown on IA-PDMS and a culture plate (Figure 2b).

The results of a Cell Counting Kit-8 (CCK-8) assay demonstrated the proliferation of hASCs on the culture plate, PDMS, and IA-PDMS at 1, 3, and 7 days (Figure 2c). Cell numbers on IA-PDMS were significantly lower than those on culture plates (control) at 1, 3, and 7 days ($p < 0.05$), whereas those on PDMS were significantly lower than those on the culture plate at 3 and 7 days ($p < 0.05$). However, although cell proliferation on IA-PDMS was significantly decreased relative to that on the culture plate, it remained significantly increased compared to that on PDMS on Days 3 and 7 ($p < 0.05$). The increased cell proliferation on IA-PDMS might be attributed to the hydrophilicity of the IA-PDMS surface, which might have inhibited protein adsorption and subsequent cell adhesion. These results were consistent with those of previous studies, which showed that hydrophilic surfaces were better at preventing protein adsorption than hydrophobic surfaces.[21,50,59,60] Figure 2d shows cell cytotoxicity results using the 3-[4,5-dimethylthiazol-2-yl]-2,5-diphenyltetrazolium bromide (MTT) assay. The PDMS and IA-PDMS samples showed significantly lower absorbance than cells on a plate at Days 1, 3, and 7 ($p < 0.05$). However, we observed increases in the absorbance of PDMS and IA-PDMS from Days 1 to 7, with that of IA-PDMS being significantly higher than that of PDMS ($p < 0.05$). This finding confirmed that cells were viable and capable of proliferation.

2.3 | Stability of IA-PDMS surface

Stability of the IA-PDMS surface was examined for up to 60 days using the water contact angle and FTIR as parameters of surface hydrophilicity stability and in vitro anti-protein adsorption, antibacterial adhesion, and cell studies as parameters of surface biocompatibility. IA-PDMS could maintain surface hydrophilicity (Figures S1b,c and S2b), as well as surface biocompatibility (Figures S4–S6), even after exposure to the air for up to 60 days. After storage in de-ionized water (DI) and Dulbecco's phosphate-buffered saline (DPBS), IA-PDMS showed better hydrophilic stability and biocompatibility than when exposed to the air. Since the in vivo environment is hydrophilic, for this modified surface, it was considered that biocompatibility in vivo was improved and could be maintained for up to 60 days. Similar results were obtained in our previous study, which showed that the hydrophilicity and biocompatibility of an oxygen (O_2) plasma-treated silicone implant surface could be maintained for up to 60 days in DI storage.[61] However, preserving a silicone implant in DI before implantation might not represent proper, realistic use, and O_2 plasma-treated implants showed unstable properties upon exposure to the air. Therefore, IA-PDMS surface modification would be a better choice for improving silicone implant surfaces, because hydrophilicity and biocompatibility could be maintained even after exposure to the air.

2.4 | Surface morphologies

Figure 2e shows the surface morphologies of PDMS and IA-PDMS, as well as those of hASCs on a cultured plate, hASC-PDMS, and hASC-IA-PDMS using scanning electron microscopy (SEM). The surfaces of PDMS and IA-PDMS were smooth, even, and clear, consistent with the results of a previous study.[21] Cells on IA-PDMS were shown to be long and widely spread on the sample surface with a copious amount of cells, exhibiting the same pattern as those on a culture plate. In contrast, cells on the PDMS surface were spherical, and their number
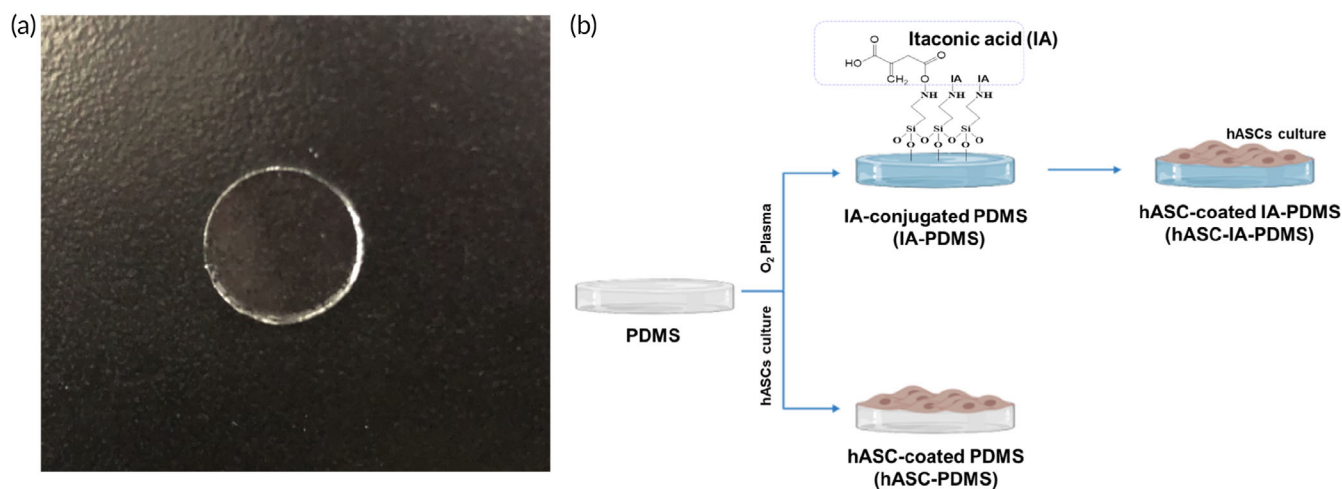
FIGURE 1 (a) Poly(dimethylsiloxane) (PDMS) membrane samples. (b) Schematic representation of the coating of a PDMS surface with human adipose-derived stem cells (hASCs), as well as PDMS-conjugated itaconic acid (IA) (150 mM) coating with hASCs

was far lower than that on the culture plate and IA-PDMS. The difference observed in cell morphology between the PDMS and IA-PDMS surfaces was attributed to the hydrophilicity of the material surfaces. A hydrophilic surface is assumed to allow cells to better attach to the surface, resulting in a long and flattened cell morphology. In contrast, a hydrophobic surface would provide smaller attachment areas on its surface, resulting in a more rounded cell morphology.[62,63]

2.5 | In vitro cytokine release

We screened for in vitro cytokine release using a proteome array and showed that the identified factors included the chemokine ligand (CCL)2, chemokine (C-X-C motif) ligand CXCL12, CXCL1, interleukin (IL)-6, IL-8, and endothelial plasminogen activator inhibitor (SERPINE1) (Figure 3). We hence noted that the cytokines released from hASCs were similar to those reported in a previous study,[64] but we observed no significant differences between the PDMS (control) and hASC-coated samples (hASC-PDMS and hASC-IA-PDMS; $p < 0.05$); however, the hASC-coated groups showed a lower pixel density for CCL2 than the control. Similarly, the pixel densities of CXCL1 and CXCL12 from hASC-PDMS and hASC-IA-PDMS were shown to be significantly lower than those of the control ($p < 0.01$). The pixel density values of IL-6 from the hASC-coated samples were also significantly lower than those of the control ($p < 0.05$), and the same was true for IL-8 ($p < 0.01$) and SERPIN E1 ($p < 0.05$).

The CCL2 chemokine, associated with CCL2/CCR2 signaling, is known to play a role in regulating the recruitment and polarization of macrophages during inflammation.[65] Likewise, CXCL1 and CXCL12 are chemokines associated with chemotaxis and inflammation,[65,66] whereas both IL-6 and IL-8 are proinflammatory factors. Previous studies reported that IL-6 induces the generation of collagen type I and plays a role in the response to infection and tissue injury.[67,68] Moreover, IL-8, one of the key mediators of the inflammatory

response, has been reported to have an important role in angiogenesis,[69,70] whereas SERPINE1 has been reported to play an important role in suppressing the adhesion, proliferation, and motility of endothelial and vascular smooth muscle cells.[71,72] Increased secretion of SERPINE1 has been observed during inflammation, physical injury, and exposure to angiotensin II. Further, SERPINE1 reportedly participates in the tissue injury repair program by inhibiting proliferation while promoting the migration of cells.[73] As such, the decreased release of these cytokines from the hASC-PDMS and hASC-IA-PDMS surfaces might further assist in reducing inflammation and increasing cell proliferation.

2.6 | In vivo experiments

Here, hASC-PDMS, IA-PDMS, and hASC-IA-PDMS groups were established as treatment groups and PDMS was established as a control group, and hASC-coated PDMS groups were referred to hASC-PDMS and hASC-IA-PDMS groups. Categorized results of these studies are as follows.

2.6.1 | mRNA gene expression

We extracted mRNA from the capsule tissue and compared the expression levels of genes related to host reactions to foreign bodies (Table S1). Our analysis was divided into four categories, namely extracellular matrix (ECM) structural constituent genes (α-smooth muscle actin [SMA], collagen 1 alpha 1 [COL1A1], and collagen 3 alpha 1 [COL3A1]), inflammation (tumor necrosis factor [TNF]-α, interleukin [IL]-1β, and IL-6), transforming growth factor [TGF]-β signaling (TGF-β1 and SMAD3), and M2 macrophage polarization-related genes (IL-13 and CCL2) (Figure 4). The thickness of the capsule was determined based on the amount of accumulated collagen. When comparing the
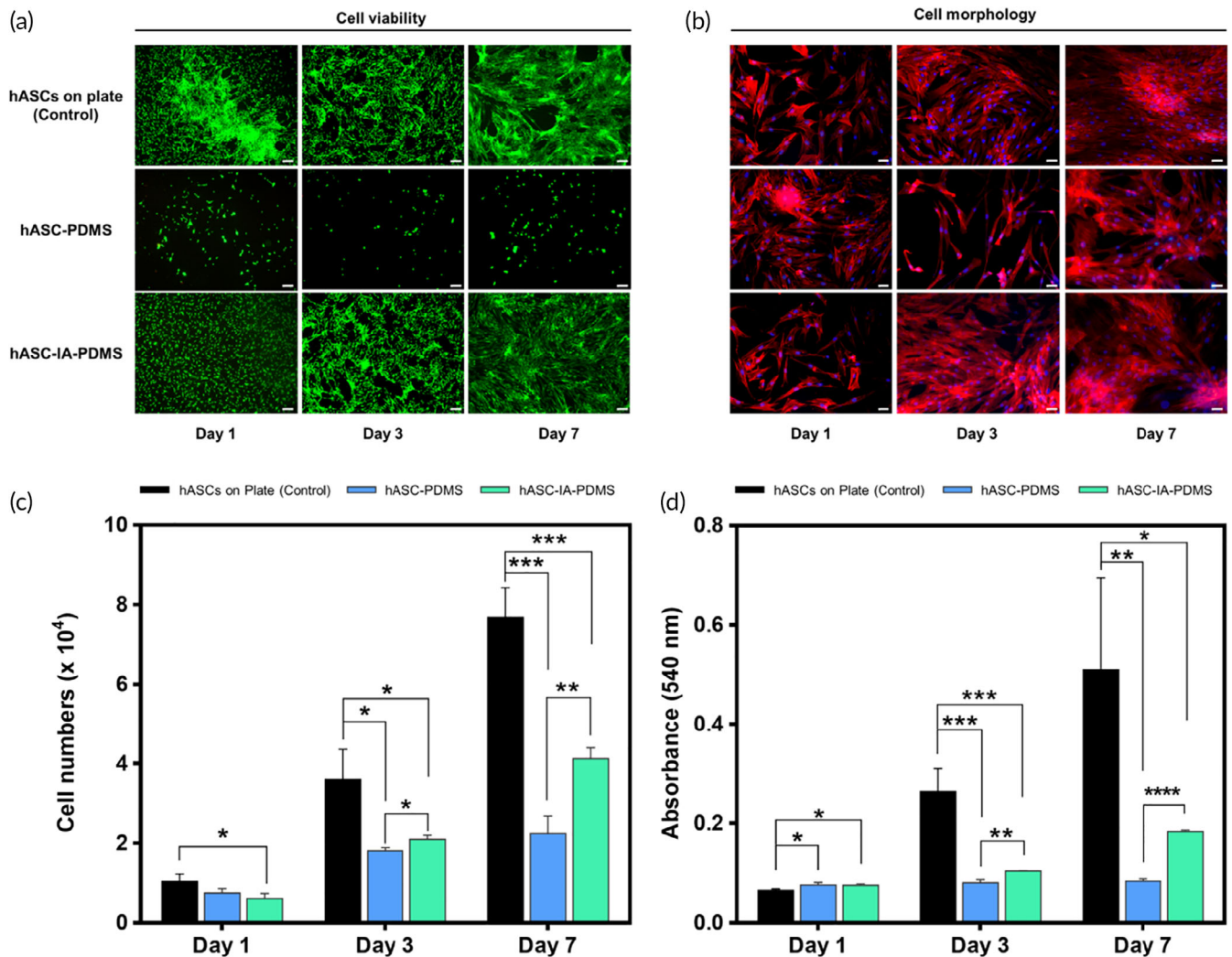
FIGURE 2 (a) Fluorescence micrograph of in vitro cell viability and (b) cell morphology of human adipose-derived stem cells (hASCs) on a plate, hASC-poly(dimethylsiloxane) (PDMS), and hASC-itaconic acid (IA)-PDMS at 1, 3, and 7 days at a magnification of 4× (for cell viability) or 10× (for cell morphology). Results of (c) cell proliferation and (d) cell cytotoxicity from the CCK-8 and MTT assay, respectively, for hASCs cultured on a culture plate, PDMS, and IA-PDMS for 1, 3, and 7 days. (e) Scanning electron microscopy (SEM) micrographs of hASCs on plates, PDMS, IA-PDMS, hASC-PDMS, and hASC-IA-PDMS at a magnification of 100×. hASCs at Day 3 were used in this evaluation. Data are shown as the mean ± SD ($n = 3$). *$p < 0.05$, **$p < 0.01$, ***$p < 0.001$, and ****$p < 0.0001$ (one-way ANOVA, Bonferroni)

expression level of genes between groups, at each time point, we observed a significant decrease in the treatment groups compared with levels in the control group. In addition, we found that the expression of α-SMA was significantly decreased in the treatment groups ($p < 0.0001$). When we investigated the expression of TNF-α, IL-1β, and IL-6 in the treatment groups at 14, 30, and 60 days, we discovered that the inflammatory cytokine-related genes were expressed at a significantly lower level compared with those in the control group ($p < 0.0001$). The TGF-β cytokine is known to be predominantly involved in fibrosis and affects the differentiation of fibroblasts into myofibroblasts.[74] Additionally, it has been reported that TGF-β-induced synthesis of α-SMA requires SMAD3. To confirm this, we compared the expression level of each of these factors and observed significantly lower expression levels of TGF-$\beta1$ and SMAD3 at 14, 30, and 60 days, with a marginally lower average expression level,

especially in the hASC-coated groups ($p < 0.0001$). Finally, we investigated CCL2 and IL-13, which are known to facilitate the differentiation of macrophages toward an M2 phenotype.[57] We observed a notable increase in the expression of IL-13 in the hASC-coated groups in the initial 14 days, whereas a significantly increased expression level of CCL2 was also shown in the hASC-PDMS group at Day 14 ($p < 0.0001$).

2.6.2 | Inflammatory response around the implant

An early stage of the cellular reaction during fibrosis development is the inflammation response, which involves several reactions comprising various inflammatory cells, such as eosinophils, neutrophils, and basophils. Inflammatory cells influence macrophage activities, result in
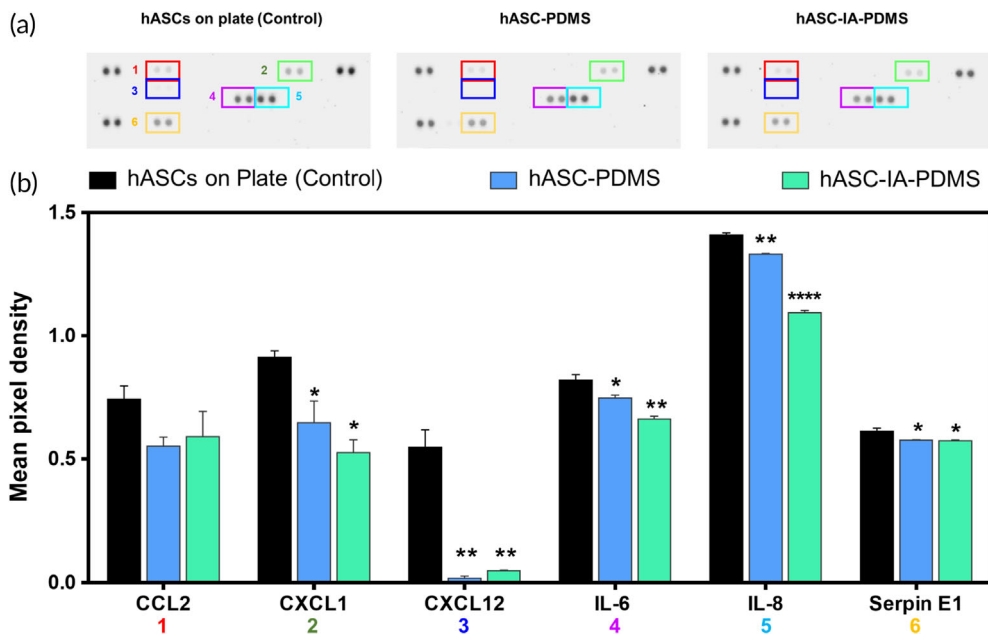
FIGURE 3 (a) Cytokine array analysis and (b) quantitative cytokine array analysis of cytokine release from human adipose-derived stem cells (hASCs) cultured on cell culture plates, poly(dimethylsiloxane) (PDMS), and IA-PDMS. hASCs at Day 3 (without changing media) were used for this evaluation. Data are shown as the mean ± SD (n = 2). *p < 0.05, **p < 0.01, and ***p < 0.0001, ****p < 0.0001 (one-way ANOVA, Bonferroni)
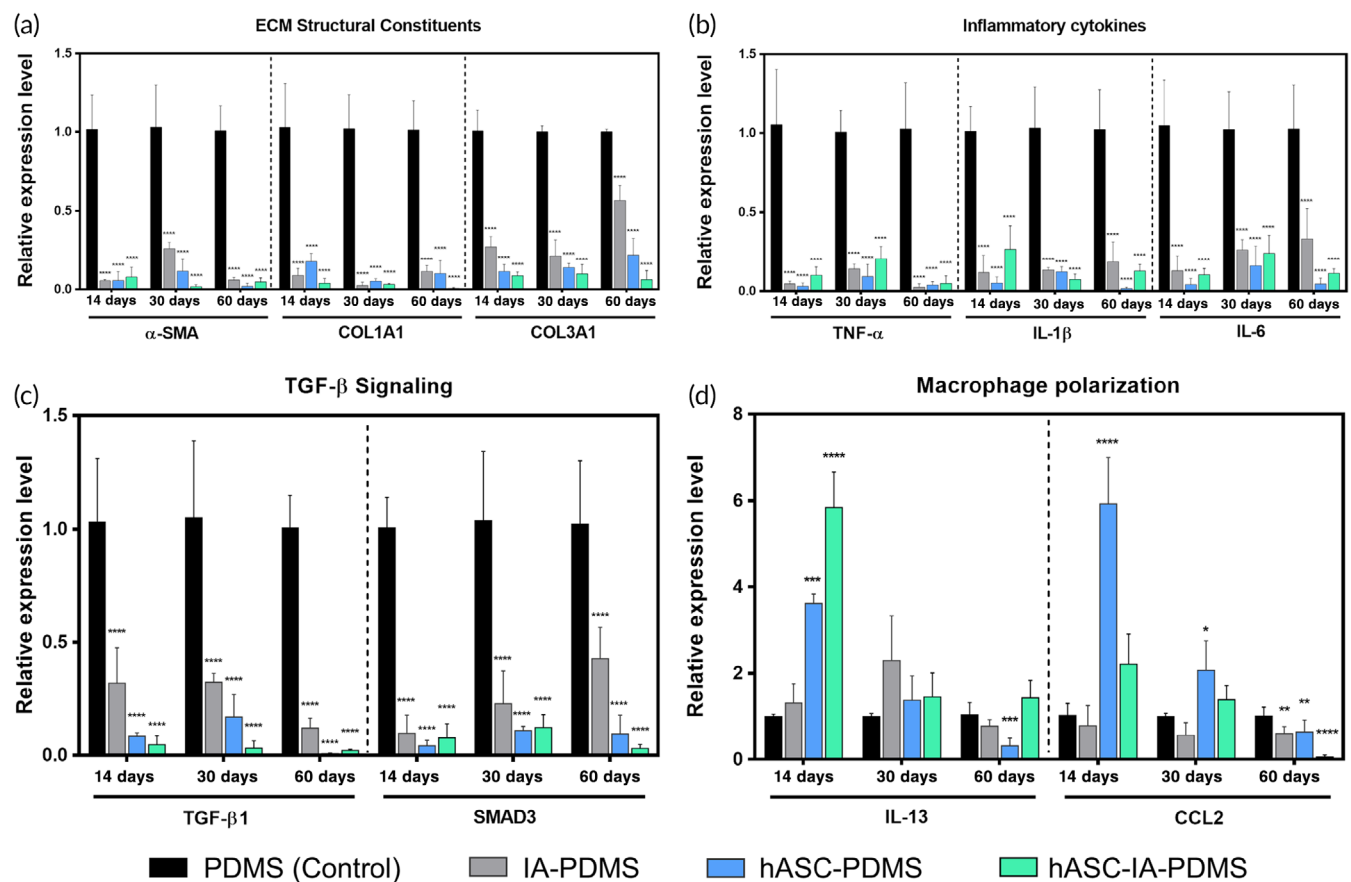
FIGURE 4 Quantitative real-time PCR analysis for the expression of various genes on the surface of poly(dimethylsiloxane) (PDMS), itaconic acid (IA)-PDMS, human adipose-derived stem cell (hASC)-PDMS, and hASC-IA-PDMS relative to the mRNA level of glyceraldehyde 3-phosphate dehydrogenase (GAPDH) at 14, 30, and 60 days after implantation. Data are shown as the mean ± SD (n = 8). **p < 0.01, ***p < 0.001, and ****p < 0.0001 (one-way ANOVA, Bonferroni)
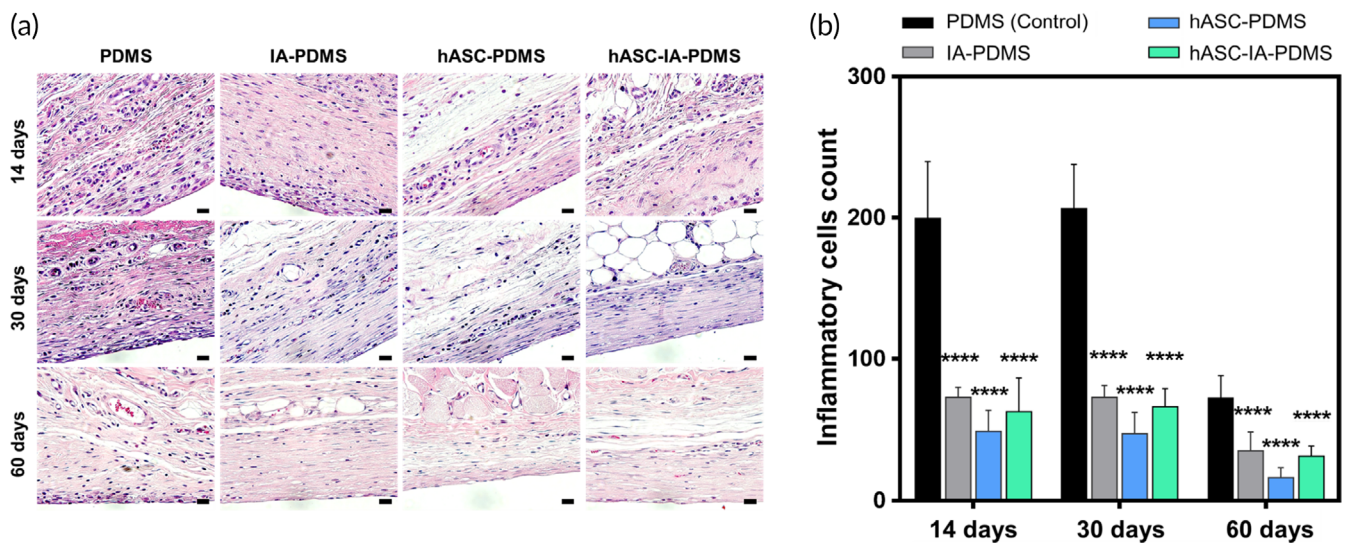
FIGURE 5 (a) Images of hematoxylin–eosin (H&E) staining of tissue slides and (b) evaluation of inflammatory cell count around implants after poly(dimethylsiloxane) (PDMS), itaconic acid (IA)-PDMS, human adipose-derived stem cell (hASC)-PDMS, and hASC-IA-PDMS implantation at 14, 30, and 60 days. Each image was obtained using optical microscopy at 400× magnification and specifically analyzed for inflammatory mediated cells (i.e., neutrophils, basophils, and eosinophils; scale bars: 20 μm). Data are shown as the mean ± SD ($n = 8$). ****$p < 0.0001$ (one-way ANOVA, Bonferroni)

fusion into foreign body giant cells, and finally create fibrosis.[45] To evaluate the inflammation occurring around the implant, we stained the tissue with hematoxylin–eosin (H&E) and evaluated the result at 14, 30, and 60 days postimplantation. As shown in Figure 5, we initially noted severe inflammation in the control group; however, the degree of inflammation was significantly reduced in the treatment groups compared with that in the control group, from the onset ($p < 0.0001$). Among the treatment groups, the degree of inflammation was lowest in the hASC-PDMS group; however, no significant difference was observed among the treatment groups at all time points ($p < 0.05$). Thus, we assumed that the surface in the treatment group was more biocompatible. The anti-inflammatory effect observed was the strongest during the early stages, with the degree of inflammation in the control group decreasing to the level of inflammation in the initial treatment group at Day 60.
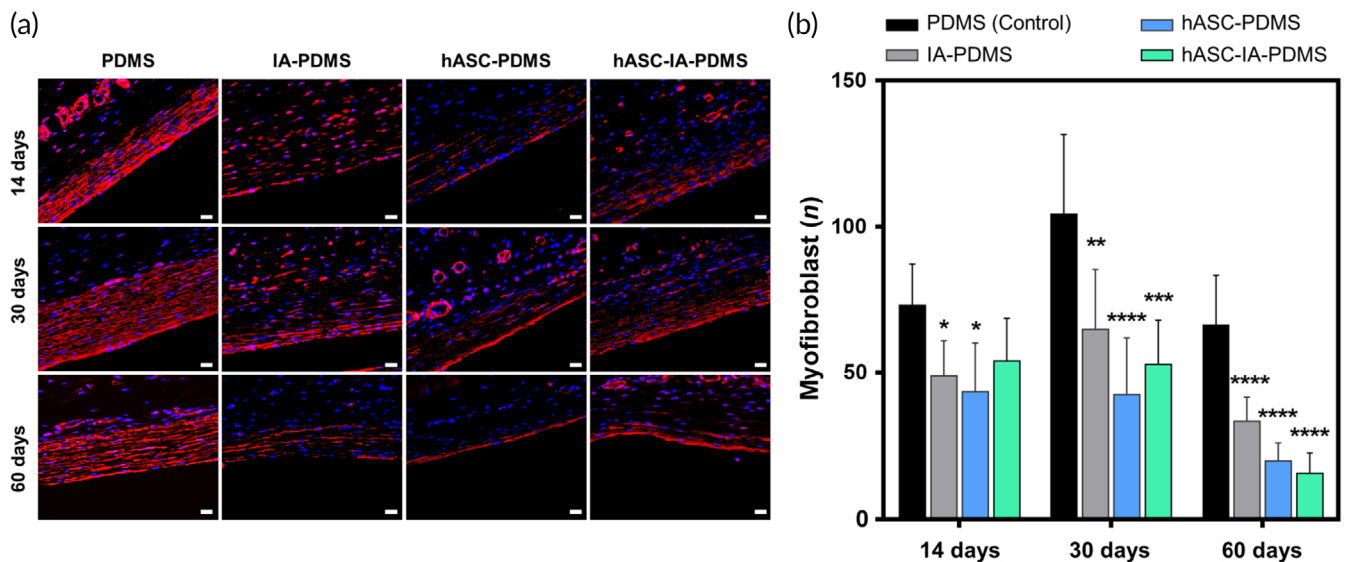
2.6.3 | Myofibroblasts

The number of myofibroblasts is commonly used as an evaluation indicator for the determination of the degree of fibrosis,[75] since more myofibroblasts present in the capsule will indicate greater contraction and therefore stronger pressure on the implant, resulting in the deformation of the implant and pain. As shown in Figure 6, myofibroblasts were primarily distributed in the region adjacent to the implant. Moreover, we noted a thicker layer of myofibroblasts in the control group than in the other groups, whereas the number of myofibroblasts in the treatment groups was significantly decreased compared with that in the control group ($p < 0.05$). This tendency was more noticeable at the 30- and 60-day time points relative to that at 14 days.
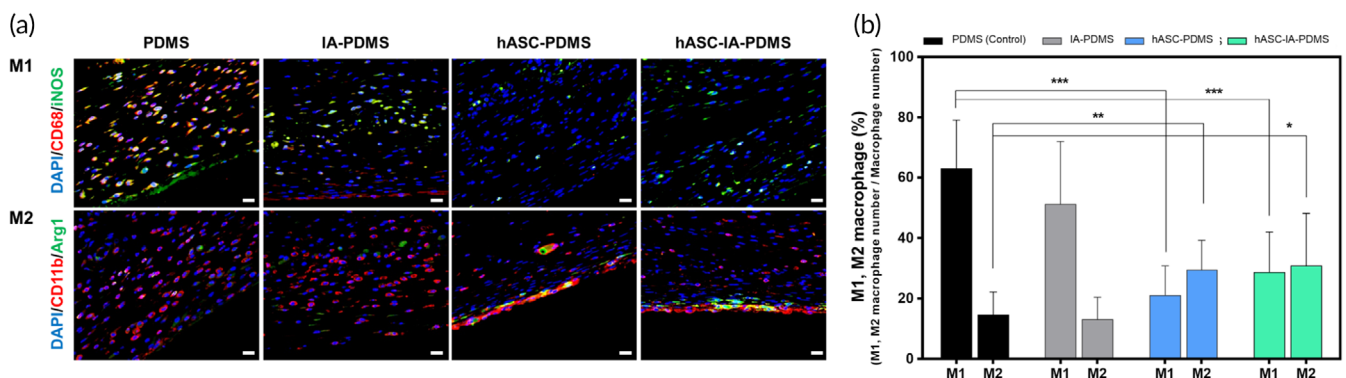
2.6.4 | Macrophages

Macrophages play an important role in the process of host reactions to foreign bodies. Monocytes can differentiate into different types of macrophages when exposed to different environments. For example, monocytes can differentiate into macrophages of the M1 (classical) and M2 (alternative) types; the M1 type primarily has a pro-inflammatory role, whereas the M2 type has anti-inflammatory and pro-healing roles.[76] We assumed that host macrophages would differentiate at different rates on each implant; thus, we analyzed their ratio by counting the number of macrophages of each type using the triple-label immunofluorescence method. We used iNOS for M1 macrophages, whereas the M2 type was stained with arginase 1. Figure 7 shows the percentage of M1 and M2 macrophages around the implants. Upon analyzing the ratio of the M1/M2 macrophages on the slide at Day 14, we detected a higher ratio of M1 macrophages in the PDMS group. The IA-PDMS group exhibited levels similar to those in the control group, but a lower percentage of M1-type macrophages was observed. However, we observed a markedly lower number of M1 macrophages in the hASC-coated groups, as well as a notable increase in the formation of M2 macrophages. This was possibly because hASCs coating affected the surrounding environment and thus the macrophage differentiation process. The presence of such an environment was evidenced by the expression level of *CCL2/IL-13* in the capsule tissue (Figure 4).

2.6.5 | Capsule thickness and collagen density

To verify the suppression of capsular contracture, we examined collagen density and capsule thickness. As shown in Figure 8a,b, a

FIGURE 6 (a) Images of immunofluorescence staining of tissue slides and (b) evaluation of the number of myofibroblasts around implants after poly(dimethylsiloxane) (PDMS), itaconic acid (IA)-PDMS, human adipose-derived stem cell (hASC)-PDMS, and hASC-IA-PDMS implantation at 14, 30, and 60 days. Each image was obtained using fluorescence microscopy at 400× magnification (scale bars: 20 μm). Data are shown as the mean ± SD ($n = 8$). *$p < 0.05$, **$p < 0.01$, ***$p < 0.0001$, and ****$p < 0.0001$ (one-way ANOVA, Bonferroni)
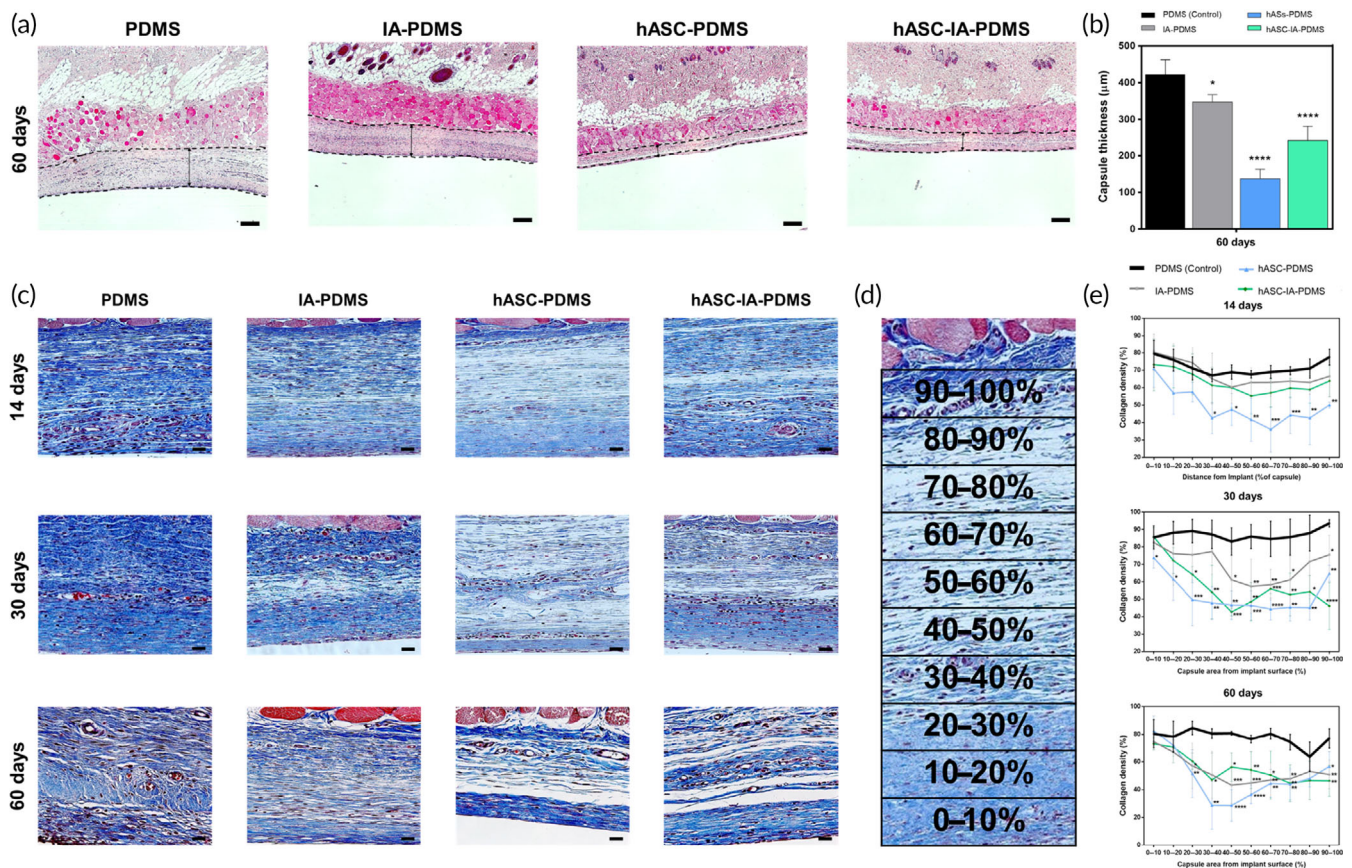

FIGURE 7 (a) Images of immunofluorescence staining of tissue slides and (b) evaluation of the percentage of M1 and M2 macrophages around implants after poly(dimethylsiloxane) (PDMS), itaconic acid (IA)-PDMS, human adipose-derived stem cell (hASC)-PDMS, and hASCs-IA-PDMS implantation at 14 days. Representative percentages of M1 and M2 macrophages were calculated based on the number of M1 or M2 macrophages divided by the total number of macrophages. Each image was obtained using fluorescence microscopy at 400× magnification (scale bars: 20 μm). Data are shown as the mean ± SD ($n = 8$). *$p < 0.05$, **$p < 0.01$, and ***$p < 0.0001$ (one-way ANOVA, Bonferroni)

significant decrease was observed in capsule thickness in the IA-PDMS group ($p < 0.05$) and the hASC-coated groups ($p < 0.0001$) compared with that in the control group at day 60. More specifically, the capsule thickness was significantly reduced in the hASC-coated groups compared with that in the IA-PDMS group, such that the hASCs coating was considered to have the ability to suppress fibrosis ($p < 0.0001$). We also observed that the lowest capsule thickness occurred on the hASC-PDMS surface and quantified the collagen density (Figure 8c,d) at each time point by determining the percentage of blue-pixel coverage in the images within 100% (at 10% intervals) of the implant–tissue interface.[77] At 14 days, in the dense capsule layer surrounding hASC-PDMS, the collagen density close to the implant

interface was >90% and was shown to decrease to approximately to 40% in the subcutaneous tissue next to the capsule (Figure 8c,d). The control group exhibited a uniform and high density on average, from the face of the implant to the muscle (0–100%). In the treatment groups, we observed lower collagen density in the middle region of the capsule. In particular, the hASC-PDMS group showed significantly lower collagen density from the initial 14 days ($p < 0.05$); the other IA-PDMS and hASC-IA-PDMS groups also showed a statistically significant decrease in density at 30 and 60 days ($p < 0.05$). Additionally, it was noted that the capsule of the hASC-PDMS group was thinner than that of the hASC-IA-PDMS group (Figure 8a). Nevertheless, qualitative and semi-qualitative determination of capsule thickness results

FIGURE 8 (a) Images of hematoxylin–eosin (H&E) staining of tissue slides and (b) evaluation of capsule thickness around implants after poly(dimethylsiloxane) (PDMS), itaconic acid (IA)-PDMS, human adipose-derived stem cell (hASC)-PDMS, and hASCs-IA-PDMS implantation at 60 days. Each image was obtained using optical microscopy at 50× magnification. Double-sided black dotted line indicates capsule thickness (scale bars: 200 μm). (c) Images of Masson's trichrome (MT) staining of tissue slides, (d) with data collected in the whole capsule area (100%) from the interface (at 10% increments), and (e) evaluation of the density of collagen deposition around implants. Collagen density was evaluated after PDMS, IA-PDMS, hASC-PDMS, and hASC-IA-PDMS implantation at 14, 30, and 60 days. Each image was obtained using optical microscopy with 400× magnification (scale bars: 20 μm). Data are shown as the mean ± SD ($n = 4$). *$p < 0.05$, **$p < 0.01$, ***$p < 0.001$, and ****$p < 0.0001$ (one-way ANOVA, Bonferroni)

could not completely refer to the degree of capsular contracture. Further, the hASC-IA-PDMS group showed superior quantitative results in the suppression of fibrosis-related gene expression in vivo (Figure 4).

We hence considered that the reduction in collagen, which is the final fibrosis product, had resulted from an inflammatory cascade that began from the initial inhibition. We assumed that the in vivo host reaction to foreign bodies was inhibited via the recognition of an environment similar to the ECM due to hASCs coating. This biocompatible surface influenced differentiation into M2, and not M1, macrophages involved in the inflammatory reaction. Thus, the healing process appeared to have started early, reducing the infiltration of immune-related cells, and resulting in the initiation of a chain reaction to detect foreign bodies. The IA-PDMS group also showed superior fibrotic suppression compared with the control group in terms of collagen density and qPCR results. However, in terms of the final cumulative amount of collagen, the capsule thickness was associated with a more pronounced difference in the hASC-coated group, possibly due to the

difference in the differentiation ratio of M1/M2 macrophages (Figure 7). In addition, these differences might have resulted not only from the biocompatibility of the implant surface but also from the effect of the cytokines secreted by the cells attached to it. Thus, we found that not only hASC-IA-PDMS was effective in reducing the formation of capsular contracture, as was hypothesized, but that hASC-PDMS also exhibited comparable anti-fibrotic ability. Further studies on the effect of cell-to-cell interactions on fibrotic reactions in these microenvironments are warranted.

3 | METHODS

3.1 | Preparation of human adipose-derived stem cells coated poly(dimethylsiloxane)

PDMS and IA-PDMS were prepared as described in the Supporting Information. PDMS and IA-PDMS samples were sterilized at 38°C for

4 h using an ethylene oxide sterilizer (SE30, ALOPS Corp., Gunpo, Korea). hASCs were cultured using Dulbecco's modified Eagle's medium low-glucose (HyClone Laboratories, Logan, UT) containing 10% fetal bovine serum (HyClone) and 1% antibiotic/antimycotic solution (HyClone). The culture media were changed every 2 days. Trypsin (0.25%; $1\times$) solution (HyClone) was used to harvest cultured cells. hASCs (2×10^4 cells) were seeded on PDMS and IA-PDMS surfaces and incubated in an incubator (HERAEUS BB 15, Thermo Fisher Scientific, Seoul, Korea) at $37°C$ with 5% CO_2. Samples with cells at 80% confluence (Day 3) were selected for use in in vivo experiments (Figure 1b). Isolation and characterization methods of hASCs are described in the Supporting Information. The use of hASCs was approved by the Chung-Ang University Hospital Institutional Review Board and conducted as specified by the guidelines of the Declaration of Helsinki (IRB No. 2151-005-463).

3.2 | Surface characterization of PDMS and IA-PDMS

To observe the surface morphologies of hASCs on plates, PDMS, IA-PDMS, hASC-PDMS, and hASC-IA-PDMS, we used SEM (S-3400 N; Hitachi, Tokyo, Japan) using a 10 kV acceleration voltage after coating with platinum layers via ion sputtering (E-1010; Hitachi) for 120 s. For samples with hASCs on the surface (hASC-PDMS and hASC-IA-PDMS), the appropriate number of cells at 80% confluence was used. The IA-PDMS was characterized using a water contact angle analyzer (Phoenix-MT, Surface Electro Optics, Suwon, Korea) and ATR/FTIR spectroscopy (Vertex 70, Bruker, MA). The surface stability of IA-PDMS was examined based on the water contact angel, ATR-FTIR, in vitro protein adsorption, in vitro anti-bacterial adhesion, and in vitro cell studies at various time intervals over 60 days, as described in the Supporting Information.

3.3 | In vitro cell cytotoxicity and characterization of cell morphology

PDMS or IA-PDMS samples with cultured cells were washed twice with DPBS (modified $1\times$, pH 7.4, HyClone) before determining in vitro cell cytotoxicity activities. The cell viability and morphology of hASCs cultured on PDMS or IA-PDMS surfaces were examined, respectively, using the LIVE/DEAD Viability/Cytotoxicity Kit for mammalian cells (Thermo Fisher, Waltham, MA) and rhodamine-phalloidin/DAPI staining at 1, 3, and 7 days. Cell adhesion and proliferation at 1, 3, and 7 days were determined using the CCK-8 assay. We also performed the MTT assay at 1, 3, and 7 days to evaluate cytocompatibility. All cell study details methods are described in the Supporting Information.

3.4 | Cytokine release

hASCs (2×10^4 cells) were cultured on culture plates (control), PDMS, and IA-PDMS in culture medium without FBS, and no media changes were performed. On Day 3, the collected supernatant was added to the Proteome Profiler™ Human Cytokine Array Kit (R&D Systems Inc., Minneapolis, MN). The cytokine assay was conducted according to the manufacturer's protocol. Chemiluminescence (ChemiDoc, Bio-Rad, CA) was used for the visualization and evaluation of protein quantities.

3.5 | In vivo experiments

For in vivo evaluation, 48 9-week-old Sprague Dawley rats (200–250 g) were used. During animal experiments, all animals were housed in a specific pathogen-free room under a 12 h day/night cycle, with free access to water and food. All experiments and the methodology used in this research were approved by the IACUC of Seoul National University Bundang Hospital (approval number: BA1903-268/015-01). To examine the antifibrotic ability of the surface-modified implants, the dorsal region of rats was completely shaved of any hair. Rats were then randomly divided into four groups of four rats each. Subsequently, incisions (2 cm in length) were made using a pair of surgical scissors. A subcutaneous pocket was made through the incision area, and the sample was inserted into the pocket. PDMS was inserted in Group 1 (control group), IA-PDMS was inserted in Group 2, hASC-PDMS was inserted in Group 3, and hASC-IA-PDMS was inserted in Group 4. In each rat, two pieces of samples were inserted parallel to the dorsal side. No DPBS washing was performed for hASC-PDMS and hASC-IA-PDMS. The incision was subsequently sutured using Nylon 4/0 (ETHILON, New Brunswick, NJ) and disinfected with betadine solution to prevent external stimulation and infection. At 14, 30, and 60 days, CO_2 euthanasia was performed for biopsy and tissue analysis. Accordingly, these tissues were collected for quantitative analysis and in vivo staining analysis. For quantitative analysis, tissues were put in a cryovial, immediately placed in liquid nitrogen, and stored at $-80°C$ until use. For in vivo staining analysis, tissues were stored in 4% formalin for 1 day. A paraffin block was subsequently prepared using biopsy tissue. Slices (thickness, 4 μm) were made and stained for each factor before tissue staining.

3.5.1 | Real-time quantitative polymerase chain reaction

Total RNA was extracted from biopsy tissue using Trizol reagent (Invitrogen, Carlsbad, CA) according to the manufacturer's instructions. Then, RNA (1 μg) was used to synthesize cDNA using the AccuPower® RocketScript™ RT-PCR PreMix & Master Mix (Bioneer, Daejeon, Korea). The synthesized cDNA was stored at $-20°C$ until use. Real-time quantitative polymerase chain reaction (RT-qPCR) analysis was performed using the Power SYBR Green PCR Master Mix (Thermo Fisher) and data analysis was performed using a StepOnePlus Real-Time PCR system (AB Applied, Life Technologies, MA). Table S2 shows the primer sequences for the glyceraldehyde 3-phosphate dehydrogenase (*GAPDH*) reference gene and target genes. The expression level of each target mRNA

was normalized to that of *GAPDH* and compared with that of the control group.

3.5.2 | Histological analysis

To confirm the efficacy of the antifibrotic functional implants, we performed histological analysis of the capsule thickness and collagen density and counts of inflammatory cells and myofibroblasts. Capsule thickness and inflammatory responses were analyzed using the H&E stain kit (H-3502; Vector Laboratories, Burlingame, CA), collagen density was analyzed using a Masson's Trichrome (MT) stain kit (Sigma-Aldrich), and myofibroblasts, a fibrotic-related factor, were analyzed using immunofluorescence staining. For capsule thickness analysis, we used H&E-stained slides to obtain $50\times$ optical microscopy tissue images, whereas capsule thickness was analyzed using at least four images per group. Capsules with the least thickness from the H&E images were selectively analyzed. For collagen density analysis, tissue images were acquired using $400\times$ optical microscopy of MT-stained slides. The blue bundle was specifically selected, and the selected area was changed into a % value relative to the total image area. All % values were objectively analyzed using ImageJ software (ver. 1.47, National Institutes of Health, Rockville, MD) in a blinded manner. Additionally, to verify the antifibrotic effect, the number of myofibroblasts was quantitatively evaluated and analyzed by immunofluorescence staining using an anti-vimentin rabbit antibody (ab92547; Abcam, Cambridge, MA) and anti-alpha smooth muscle actin mouse antibody (ab7817; Abcam) for selectivity. Each antibody was diluted at a ratio of 1:200 (vimentin) and 1:100 (alpha-smooth muscle actin), and 1:2000-diluted secondary antibodies (Alexa Fluor 488 rabbit anti-mouse IgG [H + L] [A11059; Thermo Fisher] and Alexa Fluor 488 goat anti-mouse IgG [H + L] [A11001; Thermo Fisher]) were used for the detection of fluorescence signals with a 1:2000 diluent solution. Analysis was performed using fluorescence microscopy, and samples were selectively analyzed based on 488 nm fluorescence signals emitted from specifically bound antibodies.

3.6 | Quantification and statistical analysis

Statistical analysis was performed using GraphPad Prism 7 (GraphPad Software, San Diego, CA). One-way ANOVA followed by Bonferroni's multiple comparison tests was performed. Technical replication was performed in triplicate for each analysis, and total *n* and SD values are shown in the figure legends. An alpha value of 0.05 was used for all statistical analyses.

4 | CONCLUSION

Herein, we attempted the surface modification of PDMS using hASCs, as well as IA, to minimize the host reactions to foreign bodies, which

appear as a side effect in the use of several medical devices. Both the in vitro and in vivo studies demonstrated that fibrosis was further suppressed on the hydrophilic surface modified with IA and hASCs compared to that with the hydrophobic bare PDMS surface. In addition, we confirmed that macrophage differentiation occurred toward the M2 phenotype in the group in which the surface of PDMS was modified using hASCs, further enhancing the antifibrotic ability in an anti-inflammatory environment. Overall, the fibrotic effect was lowest in hASC-PDMS and hASC-IA-PDMS, based on the following factors: capsule thickness, collagen density, and number of myofibroblasts and fibroblasts. This suggested that this cell coating had outstanding antifibrotic ability. Through these results, we have provided insights into future surface modification approaches to reduce the capsular contraction of medical devices. In future work, investigating clinical oncology might prove important.

AUTHOR CONTRIBUTIONS
Chanutchamon Sutthiwanjampa: Data curation (lead); formal analysis (lead); investigation (lead); methodology (lead); visualization (lead); writing – original draft (lead); writing – review and editing (lead). **Byung Ho Shin:** Data curation (equal); formal analysis (equal); investigation (equal); methodology (lead); writing – original draft (lead); writing – review and editing (equal). **Na Eun Ryu:** Formal analysis (equal); methodology (equal). **Shin Hyuk Kang:** Project administration (equal); supervision (supporting); validation (supporting). **Chan Yeong Heo:** Conceptualization (equal); funding acquisition (lead); project administration (lead); supervision (equal); validation (lead); writing – review and editing (supporting). **Hansoo Park:** Conceptualization (lead); funding acquisition (lead); project administration (lead); supervision (lead); validation (lead); writing – review and editing (equal).

CONFLICT OF INTERESTS
The authors declare no conflict of interest.

PEER REVIEW
The peer review history for this article is available at https://publons.com/publon/10.1002/btm2.10260.

DATA AVAILABILITY STATEMENT
The data that support the findings of this study are available from the corresponding author upon reasonable request.

ORCID
Hansoo Park https://orcid.org/0000-0002-3125-7680

REFERENCES

1. Puskas JE, Foreman-Orlowski EA, Lim GT, et al. A nanostructured carbon-reinforced polyisobutylene-based thermoplastic elastomer. *Biomaterials*. 2010;31(9):2477-2488. https://doi.org/10.1016/j.biomaterials.2009.12.003

2. Barnsley GP, Sigurdson LF, Barnsley SE, Barnsley SE. Textured surface breast implants in the prevention of capsular contracture among breast augmentation patients: a meta-analysis of randomized controlled trials. *Plast Reconstr Surg*. 2006;117(7):2182-2190.

3. Henriksen TF, Fryzek JP, Hölmich LR, et al. Surgical intervention and capsular contracture after breast augmentation: a prospective study of risk factors. *Ann Plast Surg*. 2005;54(4):343-351. https://doi.org/10.1097/01.sap.0000151459.07978.fa

4. Malata CM, Feldberg L, Coleman DJ, Foo IT, Sharpe DT. Textured or smooth implants for breast augmentation? Three year follow-up of a prospective randomised controlled trial. *Br J Plast Surg*. 1997;50(2):99-105. https://doi.org/10.1016/S0007-1226(97)91320-5

5. Schaub TA, Ahmad J, Rohrich RJ. Capsular contracture with breast implants in the cosmetic patient: saline versus silicone–a systematic review of the literature. *Plast Reconstr Surg*. 2010;126(6):2140-2149. https://doi.org/10.1097/PRS.0b013e3181f2b5a2

6. Adams WP. Capsular contracture: what is it? What causes it? How can it be prevented and managed? *Clin Plast Surg*. 2009;36(1):119-126. https://doi.org/10.1016/j.cps.2008.08.007

7. Anderson JM, Rodriguez A, Chang DT. Foreign body reaction to biomaterials. *Semin Immunol*. 2008;20(2):86-100. https://doi.org/10.1016/j.smim.2007.11.004

8. Franz S, Rammelt S, Scharnweber D, Simon JC. Immune responses to implants – a review of the implications for the design of immunomodulatory biomaterials. *Biomaterials*. 2011;32(28):6692-6709. https://doi.org/10.1016/j.biomaterials.2011.05.078

9. Shiffman MA. *Breast Augmentation*. 1st ed. Springer-Verlag; 2009:205.

10. Zeplin PH, Larena-Avellaneda A, Schmidt K. Surface modification of silicone breast implants by binding the antifibrotic drug halofuginone reduces capsular fibrosis. *Plast Reconstr Surg*. 2010;126(1):266-274. https://doi.org/10.1097/PRS.0b013e3181dbc313

11. Lin G, Zhang X, Kumar SR, Mark JE. Modification of polysiloxane networks for biocompatibility. *Mol Cryst Liq Cryst*. 2010;521(1):56-71. https://doi.org/10.1080/15421401003719738

12. Kim H, Choi W, Lee S, et al. Synthesis of biomembrane-mimic polymers with various phospholipid head groups. *Polymer*. 2014;55(2):517-524. https://doi.org/10.1016/j.polymer.2013.12.020

13. Birajdar MS, Joo H, Koh W-G, Park H. Natural bio-based monomers for biomedical applications: a review. *Biomater Res*. 2021;25(1):1-14.

14. Okabe M, Lies D, Kanamasa S, Park EY. Biotechnological production of itaconic acid and its biosynthesis in Aspergillus terreus. *Appl Microbiol Biotechnol*. 2009;84(4):597-606. https://doi.org/10.1007/s00253-009-2132-3

15. Bajpai SK, Saggu SS. Water uptake behavior of poly(methacrylamide-co-N-vinyl-2-pyrrolidone-co-itaconic acid) as pH-sensitive dydrogels: part I. *J Macromo Sci A*. 2006;43(8):1135-1150. https://doi.org/10.1080/10601320600735116

16. Patil DM, Phalak GA, Mhaske ST. Design and synthesis of bio-based UV curable PU acrylate resin from itaconic acid for coating applications. *Des Monomers Polym*. 2017;20(1):269-282. https://doi.org/10.1080/15685551.2016.1231045

17. Yang M-R, Chen K-S, Tsai J-C, Tseng C-C, Lin S-F. The antibacterial activities of hydrophilic-modified nonwoven PET. *Mater Sci Eng C*. 2002;20(1):167-173. https://doi.org/10.1016/S0928-4931(02)00028-0

18. Marcelo G, Ferreira IC, Viveiros R, Casimiro T. Development of itaconic acid-based molecular imprinted polymers using supercritical fluid technology for pH-triggered drug delivery. *Int J Pharm*. 2018;542(1):125-131. https://doi.org/10.1016/j.ijpharm.2018.03.010

19. Tomić SL, Mićić MM, Đokić D, Vasiljević-Radović DG, Filipović JM, Suljovrujić EH. Preparation of silver(I) complexes with itaconic acid-based hydrogels for biomedical application. *Mater Manuf Process*. 2009;24(10–11):1197-1201. https://doi.org/10.1080/10426910903022247

20. Michelucci A, Cordes T, Ghelfi J, et al. Immune-responsive gene 1 protein links metabolism to immunity by catalyzing itaconic acid production. *Proc Natl Acad Sci U S A*. 2013;110(19):7820-7825. https://doi.org/10.1073/pnas.1218599110

21. Birajdar MS, Cho H, Seo Y, Choi J, Park H. Surface conjugation of poly(dimethyl siloxane) with itaconic acid-based materials for antibacterial effects. *Appl Surf Sci*. 2018;437:245-256. https://doi.org/10.1016/j.apsusc.2017.12.125

22. Birajdar MS, Kim BH, Sutthiwanjampa C, Kang SH, Heo CY, Park H. Inhibition of capsular contracture of poly (dimethyl siloxane) medical implants by surface modification with itaconic acid conjugated gelatin. *J Ind Eng Chem*. 2020;89:128-138. https://doi.org/10.1016/j.jiec.2020.03.036

23. Bressan E, Botticelli D, Sivolella S, et al. Adipose- derived stem cells as a tool for dental implant osseointegration: an experimental study in the dog. *Int J Mol Cell Med*. 2015;4(4):197-208.

24. Mizuno H, Tobita M, Ogawa R, et al. *Chapter 32 - Adipose-Derived Stem Cells in Regenerative Medicine*. 3rd ed. Academic Press; 2017:459-479.

25. Mizuno H, Hyakusoku H. Fat grafting to the breast and adipose-derived stem cells: recent scientific consensus and controversy. *Aesthet Surg J*. 2010;30(3):381-387. https://doi.org/10.1177/1090820X10373063

26. Frazier TP, McLachlan JB, Gimble JM, Tucker HA, Rowan BG. Human adipose-derived stromal/stem cells induce functional CD4+ CD25+ FoxP3+ CD127-regulatory T cells under low oxygen culture conditions. *Stem Cells Dev*. 2014;23(9):968-977. https://doi.org/10.1089/scd.2013.0152

27. Wang Y, Liu J, Jiang Q, et al. Human adipose-derived mesenchymal stem cell-secreted CXCL1 and CXCL8 facilitate breast tumor growth by promoting angiogenesis. *Stem Cells*. 2017;35(9):2060-2070. https://doi.org/10.1002/stem.2643

28. O'Halloran N, Courtney D, Kerin MJ, Lowery AJ. Adipose-derived stem cells in novel approaches to breast reconstruction: their suitability for tissue engineering and oncological safety. *Breast Cancer (Auckl)*. 2017;11:1178223417726777. https://doi.org/10.1177/1178223417726777

29. Tsekouras A, Mantas D, Tsilimigras DI, Ntanasis-Stathopoulos I, Kontos M, Zografos GC. Adipose-derived stem cells for breast reconstruction after breast surgery - preliminary results. *Case Rep Plast Surg Hand Surg*. 2017;4(1):35-41. https://doi.org/10.1080/23320885.2017.1316201

30. Moioli EK, Chen M, Yang R, Shah B, Wu J, Mao JJ. Hybrid adipogenic implants from adipose stem cells for soft tissue reconstruction *in vivo*. *Tissue Eng Part A*. 2010;16(11):3299-3307. https://doi.org/10.1089/ten.TEA.2010.0157

31. Collins E, Gu F, Qi M, et al. Differential efficacy of human mesenchymal stem cells based on source of origin. *J Immunol*. 2014;193(9):4381. https://doi.org/10.4049/jimmunol.1401636

32. Abumaree M, Al Jumah M, Pace RA, Kalionis B. Immunosuppressive properties of mesenchymal stem cells. *Stem Cell Rev Rep*. 2012;8(2):375-392. https://doi.org/10.1007/s12015-011-9312-0

33. Singer NG, Caplan AI. Mesenchymal stem cells: mechanisms of inflammation. *Annu Rev Pathol*. 2011;6(1):457-478. https://doi.org/10.1146/annurev-pathol-011110-130230

34. Caliogna L, Bina V, Botta L, et al. Osteogenic potential of human adipose derived stem cells (hASCs) seeded on titanium trabecular spinal cages. *Sci Rep*. 2020;10(1):18284. https://doi.org/10.1038/s41598-020-75385-y

35. Yoshida Y, Matsubara H, Fang X, et al. Adipose-derived stem cell sheets accelerate bone healing in rat femoral defects. *PLoS*

One. 2019;14(3):e0214488. https://doi.org/10.1371/journal.pone.0214488

36. Barr S, Hill E, Bayat A. Development, fabrication and evaluation of a novel biomimetic human breast tissue derived breast implant surface. *Acta Biomater.* 2017;49:260-271.

37. Sangkum P, Yafi FA, Kim H, et al. Effect of adipose tissue-derived stem cell injection in a rat model of urethral fibrosis. *Can Urol Assoc J.* 2016;10(5–6):E175.

38. Dunham C, Havlioglu N, Chamberlain A, Lake S, Meyer G. Adipose stem cells exhibit mechanical memory and reduce fibrotic contracture in a rat elbow injury model. *FASEB J.* 2020;34(9):12976-12990.

39. Almadori A, Griffin M, Ryan CM, et al. Stem cell enriched lipotransfer reverses the effects of fibrosis in systemic sclerosis. *PLoS One.* 2019;14(7):e0218068.

40. Thomé J, Diehm YF, Will P, et al. Stem-cell enriched hybrid breast reconstruction and augmentation and its effects on capsular contracture. *Senologie-Zeitschrift für Mammadiagnostik und-therapie.* 2021;18(02):97.

41. Kutner N, Kunduru KR, Rizik L, Farah S. Recent advances for improving functionality, biocompatibility, and longevity of implantable medical devices and deliverable drug delivery systems. *Adv Funct Mater.* 2021;2010929. https://doi.org/10.1002/adfm.202010929

42. Josyula A, Parikh KS, Pitha I, Ensign LM. Engineering biomaterials to prevent post-operative infection and fibrosis. *Drug Deliv Transl Res.* 2021;11:1-14.

43. Nam S-Y, Ji HB, Shin BH, et al. Silicone breast implant coated with triamcinolone inhibited breast-implant-induced fibrosis in a porcine model. *Materials.* 2021;14(14):3917.

44. Kang SH, Sutthiwanjampa C, Heo CY, Kim WS, Lee S-H, Park H. Current approaches including novel nano/microtechniques to reduce silicone implant-induced contracture with adverse immune uesponses. *Int J Mol Sci.* 2018;19(4):1171. https://doi.org/10.3390/ijms19041171

45. Shin BH, Kim BH, Kim S, Lee K, Choy YB, Heo CY. Silicone breast implant modification review: overcoming capsular contracture. *Biomater Res.* 2018;22:37-37. https://doi.org/10.1186/s40824-018-0147-5

46. Yeo LY, Chang H-C, Chan PPY, Friend JR. Microfluidic devices for bioapplications. *Small.* 2011;7(1):12-48. https://doi.org/10.1002/smll.201000946

47. Andersson H, van den Berg A. Microfluidic devices for cellomics: a review. *Sens Actuators B Chem.* 2003;92(3):315-325. https://doi.org/10.1016/S0925-4005(03)00266-1

48. Lee E, Yang S, Jung J, Oh J. Polydimethylsiloxane-assisted control of platelet attachment for rapid activation. *Dig J Nanomater Biostruct.* 2015;10(3):565-870.

49. Park JU, Ham J, Kim S, et al. Alleviation of capsular formations on silicone implants in rats using biomembrane-mimicking coatings. *Acta Biomater.* 2014;10(10):4217-4225. https://doi.org/10.1016/j.actbio.2014.07.007

50. Lee JS, Shin BH, Yoo BY, et al. Modulation of foreign body reaction against PDMS implant by grafting topographically different poly(acrylic acid) micropatterns. *Macromol Biosci.* 2019;19(12):1900206. https://doi.org/10.1002/mabi.201900206

51. Jensen C, Gurevich L, Patriciu A, Struijk JJ, Zachar V, Pennisi CP. Increased connective tissue attachment to silicone implants by a water vapor plasma treatment. *J Biomed Mater Res A.* 2012;100A(12):3400-3407. https://doi.org/10.1002/jbm.a.34284

52. Kang S, Kim J, Kim S, et al. Efficient reduction of fibrous capsule formation around silicone breast implants densely grafted with 2-methacryloyloxyethyl phosphorylcholine (MPC) polymers by heat-induced polymerization. *Biomater Sci.* 2020;8(6):1580-1591. https://doi.org/10.1039/C9BM01802F

53. Thitilertdecha P, Lohsiriwat V, Poungpairoj P, Tantithavorn V, Onlamoon N. Extensive characterization of mesenchymal stem cell marker expression on freshly isolated and *in vitro* expanded human adipose-derived stem cells from breast cancer patients. *Stem Cells Int.* 2020;2020:8237197. https://doi.org/10.1155/2020/8237197

54. Suto EG, Mabuchi Y, Toyota S, et al. Advantage of fat-derived CD73 positive cells from multiple human tissues, prospective isolated mesenchymal stromal cells. *Sci Rep.* 2020;10(1):15073. https://doi.org/10.1038/s41598-020-72012-8

55. Zhu Y-Z, Hu X, Zhang J, Wang Z-H, Wu S, Yi Y-Y. Extracellular vesicles derived from human adipose-derived stem cell prevent the formation of hypertrophic scar in a rabbit model. *Ann Plast Surg.* 2020;84(5):602-607. https://doi.org/10.1097/SAP.0000000000002357

56. Spiekman M, van Dongen JA, Willemsen JC, Hoppe DL, van der Lei B, Harmsen MC. The power of fat and its adipose-derived stromal cells: emerging concepts for fibrotic scar treatment. *J Tissue Eng Regen Med.* 2017;11(11):3220-3235. https://doi.org/10.1002/term.2213

57. Song K, Li l, Yan X, et al. Characterization of human adipose tissue-derived stem cells *in vitro* culture and *in vivo* differentiation in a temperature-sensitive chitosan/β- glycerophosphate/collagen hybrid hydrogel. *Mater Sci Eng C.* 2017;70:231-240. https://doi.org/10.1016/j.msec.2016.08.085

58. Devitt SM, Carter CM, Dierov R, Weiss S, Gersch RP, Percec I. Successful isolation of viable adipose-derived stem cells from human adipose tissue subject to long-term cryopreservation: positive implications for adult stem cell-based therapeutics in patients of advanced age. *Stem Cells Int.* 2015;2015:146421. https://doi.org/10.1155/2015/146421

59. Xia X-K, Wang X-H, Zhang W, Han X-L, Chen P, Jiang Y. Improving the wettability and antiprotein adsorption property of PDMS by swelling–deswelling approach. *J Coat Technol Res.* 2019;16(2):353-361. https://doi.org/10.1007/s11998-018-0070-7

60. Joo H, Park J, Sutthiwanjampa C, et al. Surface coating with hyaluronic acid-gelatin-crosslinked hydrogel on gelatin-conjugated poly(dimethylsiloxane) for implantable medical device-induced fibrosis. *Pharmaceutics.* 2021;13(2):269.

61. Kang SH, Sutthiwanjampa C, Kim HS, et al. Optimization of oxygen plasma treatment of silicone implant surface for inhibition of capsular contracture. *J Ind Eng Chem.* 2021;97:226-238. https://doi.org/10.1016/j.jiec.2021.02.004

62. Argentati C, Morena F, Montanucci P, et al. Surface hydrophilicity of poly(l-lactide) acid polymer film changes the human adult adipose stem cell architecture. *Polymers (Basel).* 2018;10(2):140. https://doi.org/10.3390/polym10020140

63. Ahn HH, Lee IW, Lee HB, Kim MS. Cellular behavior of human adipose-derived stem cells on wettable gradient polyethylene surfaces. *Int J Mol Sci.* 2014;15(2):2075-2086. https://doi.org/10.3390/ijms15022075

64. Yeh W-L, Tsai C-F, Chen D-R. Peri-foci adipose-derived stem cells promote chemoresistance in breast cancer. *Stem Cell Res Ther.* 2017;8(1):177-177. https://doi.org/10.1186/s13287-017-0630-2

65. Yao M, Brummer G, Acevedo D, Cheng N. *Chapter Eight - Cytokine Regulation of Metastasis and Tumorigenicity.* 1st ed. Academic Press; 2016:265-367.

66. Singhal G, Baune BT. *Chapter 8 - Do Chemokines Have a Tole in the Pathophysiology of Depression?.* 1st ed. Academic Press; 2018:135-159.

67. Bou-Gharios G, de Crombrugghe B. *Chapter 15 - Type I Collagen Structure, Synthesis, and Regulation.* 3rd ed. Academic Press; 2008:285-318.

68. Tanaka T, Narazaki M, Kishimoto T. IL-6 in inflammation, immunity, and disease. *Cold Spring Harb Perspect Biol.* 2014;6(10):a016295. https://doi.org/10.1101/cshperspect.a016295

69. Brat DJ, Bellail AC, Van Meir EG. The role of interleukin-8 and its receptors in gliomagenesis and tumoral angiogenesis. *Neuro Oncol.* 2005;7(2):122-133. https://doi.org/10.1215/S1152851704001061

70. Bishara N. *Chapter 18 - the Use of Biomarkers for Detection of Early- and Late-Onset Neonatal Sepsis.* 2nd ed. Saunders; 2012:303-315.

71. Czekay R-P, Simone TM, Higgins PJ. *SerpinE1.* 1st ed. Springer; 2017:1-11.

72. Wu J, Strawn TL, Luo M, et al. Plasminogen activator inhibitor-1 inhibits angiogenic signaling by uncoupling vascular endothelial growth factor receptor-2-αVβ3 integrin cross talk. *Arterioscler Thromb Vasc Biol.* 2015;35(1):111-120.

73. Simone TM, Higgins CE, Czekay R-P, et al. SERPINE1: a molecular switch in the proliferation-migration dichotomy in wound-"activated" keratinocytes. *Adv Wound Care (New Rochelle).* 2014;3(3):281-290. https://doi.org/10.1089/wound.2013.0512

74. X-m M, Nikolic-Paterson DJ, Lan HY. TGF-β: the master regulator of fibrosis. *Nat Rev Nephrol.* 2016;12(6):325-338. https://doi.org/10.1038/nrneph.2016.48

75. Bochaton-Piallat M-L, Gabbiani G, Hinz B. The myofibroblast in wound healing and fibrosis: answered and unanswered questions. *F1000Res.* 2016;5:752. https://doi.org/10.12688/f1000research.8190.1

76. Sridharan R, Cameron AR, Kelly DJ, Kearney CJ, O'Brien FJ. Biomaterial based modulation of macrophage polarization: a review and suggested design principles. *Mater Today.* 2015;18(6):313-325. https://doi.org/10.1016/j.mattod.2015.01.019

77. Zhang L, Cao Z, Bai T, et al. Zwitterionic hydrogels implanted in mice resist the foreign-body reaction. *Nat Biotechnol.* 2013;31(6):553-556. https://doi.org/10.1038/nbt.2580

SUPPORTING INFORMATION

Additional supporting information may be found in the online version of the article at the publisher's website.